

The Solid Solution and Grain Boundary Hardening due to Mg in an Aluminum Alloy System at Room and Elevated Temperatures



H. JIN

The solid solution and grain boundary hardening due to Mg in Al-1.5wt pct Mn-0.5wt pct Cu system with 0.1 to 2.1 wt pct Mg has been studied at 25 °C to 345 °C. A transition temperature around 200 °C was found, while below it, the frictional stress, solid solution hardening from Mg and grain boundary hardening are little affected by temperature. This is due to the enhanced solute pinning on dislocations, by Cottrell clouds or other extensive segregation of solutes to dislocations. Above the transition, the solid solution hardening is controlled by the temperature-dependent shear modulus, which decreases linearly with the increasing temperature up to ~ 300 °C. Therefore, both the frictional stress and the solution hardening from Mg decrease linearly with the increasing temperature above ~ 200 °C. The grain boundary hardening obeys the Hall–Petch equation over the whole temperature range. Below the transition point the Petch slope is mainly controlled by the solute Mg, while above this temperature it is dependent on both the solute Mg level and temperature. The Petch slope increases linearly with solute Mg level, and decreases proportionally with the inverse of temperature. Semiempirical expressions for the yield strength at 25 °C to 345 °C were derived, including both solid solution and grain boundary effects.

<https://doi.org/10.1007/s11661-018-4949-9>

© Her Majesty the Queen in Right of Canada, as represented by the Minister of Natural Resources 2018

I. INTRODUCTION

MAGNESIUM is the most critical alloying element for solid solution hardening in aluminum alloys, due to its high solid solubility and high lattice misfit in the aluminum matrix.^[1–4] The solid solution hardening effect of Mg has been studied extensively for decades, especially in Al-Mg-Mn and Al-Mg-Cr sheet products for structural applications. Since these alloys were initially designed for cold-forming and room-temperature services, the investigations are mainly performed at room temperatures only. Moreover, the experimental results are often inconsistent; for example, the increase of yield strength (YS) per 1 at. pct Mg in fully annealed temper has been reported to vary from 14 to 27 MPa at room temperature.^[5–9] Other strengthening mechanisms are unavoidably involved, especially grain boundary hardening, because Mg has a strong grain-refinement effect for recrystallized grain structures.^[8,9]

Al-1.5 wt pct Mn-0.5 wt pct Cu alloy has been widely used as the core alloy in brazing sheets for automotive heat exchangers. The YS is about 50 to 65 MPa with the service temperature up to ~ 150 °C, and it drops quickly at higher temperatures, especially above 200 °C.^[10–12] Since super/turbo-charged engines become popular for better fuel efficiency and lower GHG emission, many heat exchangers may work at the temperature range from 200 °C to 300 °C, while the conventional Al-Mn-Cu alloys become too soft. It was found in a previous study that the addition of Mg significantly improves the high-temperature strength of Al-Mn-Cu alloys, but it was unclear whether the strengthening is due to the solid solution solely or to the combination of solid solution and grain boundaries.^[12] Hence, in the current study, the strengthening of Mg was systemically investigated in Al-Mn-Cu-Mg system from the room temperature up to 345 °C. An attempt was made to separate the solid solution and grain boundary effects, and to derive semiempirical expressions that include both effects as a function of Mg level and temperature.

II. EXPERIMENTS

Five Al-1.5 wt pct Mn-0.5 wt pct Cu alloys with the increasing Mg contents of 0.1, 0.5, 1.0, 1.5, and 2.1 wt pct, labeled Alloys-1 to 5 (Table I), were made by direct

H. JIN is with the CanmetMATERIALS, Natural Resources Canada, Hamilton, Ontario L8P 0A5, Canada. Contact e-mail: haiou.jin@canada.ca

Manuscript submitted April 13, 2018.

Article published online October 16, 2018

chill casting. The ingot dimension was 610mm by 229mm by 95mm. They were scalped ~ 10 mm on each rolling face, re-heated to 520 °C, soaked for ~ 7 hours, and hot rolled to ~ 5mm with exit temperature ranging from 280 °C to 295 °C, which is below the recrystallization temperature. The hot band was cold rolled down to 2.5, 1, and 0.5mm, corresponding to ~ 50, 80, and 90 pct thickness reductions, respectively. Tensile specimens were machined from the hot bands and the cold-rolled sheets along the rolling direction (RD).

To obtain a wide range of fully recrystallized grain sizes, the tensile specimens were heat treated variously: flash annealing at 525 °C to 600 °C for 5 to 10 minutes or batch annealing at 500 °C to 520 °C for 0.5 to 2 hours. In flash annealing, the heating up was completed within 2 minutes, while in batch annealing the heating rate was only 50 °C/h. After annealing the specimens were quenched to room temperature by forced air. It was intended to make fine grain structures by heavy rolling reduction, high heating rate and short soaking time, and coarse ones by limited rolling reduction, slow heating rate and long soaking time. The annealing temperature and soaking time were carefully chosen to avoid changes of Mg, Mn or Cu levels in solid solution or the number and size of dispersoid particles.

The tensile properties were determined with a constant cross-head speed of 0.75 mm/min, equivalent to $2 \times 10^{-3} \text{ s}^{-1}$ initial strain rate, at 25 °C, 100 °C, 177 °C, 215 °C, 235 °C, 260 °C, 288 °C, 320 °C, and 345 °C in a heating chamber. Except for room temperature testing, the chamber was preheated, and it took less than 20 minutes for the specimen to reach the testing temperature. At each temperature, three specimens were tested and the mean values of YS were recorded. The microstructures were examined by Olympus PMG3 optical microscope and Philips XL30 scanning electron microscope (SEM). The intermetallic phases were identified and analyzed by energy dispersive X-ray (EDX) in SEM. The mean grain sizes were measured in the sheet longitudinal section by line intercept method along the RD in SEM backscatter images, with at least 200 grain boundaries counted for each sample. The metallographic specimens were prepared by mechanical polishing with diamond pastes down to 3 μm , followed by mechanical-chemical polish in a Buehler Vibromet polisher using 0.5 μm colloidal silica for at least 4 hours.

Table I. Chemical Compositions of the Five Al-Mn-Cu Alloys, in Weight Percent Except for Mg Where Both Weight Percent and Atomic Fraction c_{Mg} Are Included

Alloy	Mn	Cu	Fe	Si	Mg		Al
					Wt Pct	c_{Mg}	
1	1.52	0.50	0.24	0.09	0.11	0.0010	balance
2	1.50	0.54	0.26	0.11	0.51	0.0045	balance
3	1.48	0.54	0.26	0.11	1.00	0.0088	balance
4	1.52	0.54	0.24	0.11	1.52	0.0133	balance
5	1.51	0.55	0.24	0.12	2.06	0.0181	balance

III. RESULTS

The intermetallic particles detected in the tensile specimens are nearly all $\text{Al}_6(\text{Mn,Fe})$, with a very few undissolved Mg_2Si . The $\text{Al}_6(\text{Mn,Fe})$ particles were either coarse constituents, several to several ten micrometers, or small dispersoids below 2 μm , *e.g.*, see Figure 1. The sizes, volume fractions and spatial distributions of the particles appear identical, regardless of the different Mg levels, rolling reductions or heat treatments. A systematic investigation of the microstructures in these alloys, especially the phase, morphology, size and distribution of the intermetallic particles, has been published earlier.^[13] All the specimens are fully recrystallized whereas the grain structures are more or less flattened and elongated along the RD, especially for the very coarse-grained specimens, *e.g.*, see Figure 2. With the increasing Mg level, rolling reduction and

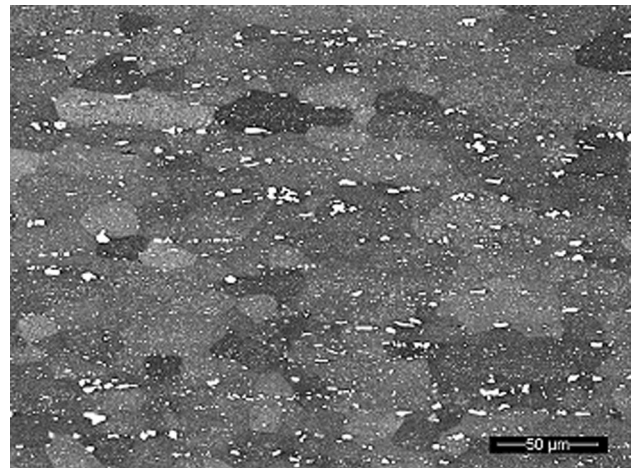


Fig. 1—SEM backscattered image showing the $\text{Al}_6(\text{Mn, Fe})$ constituent and dispersoid particles in the longitudinal section of 1 mm Alloy-5 sheet after flash annealing at 600 °C for 5 min. The RD is horizontal and the thickness direction is vertical.

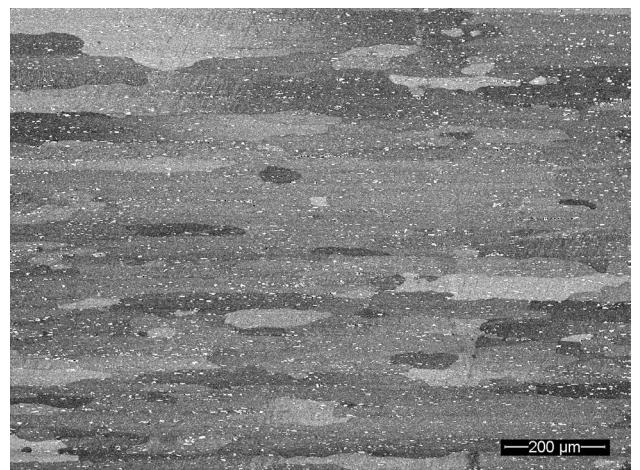


Fig. 2—SEM backscattered image showing the grain structure in the longitudinal section of 5 mm Alloy-2 hot band after batch annealing at 520 °C for 2 h. The RD is horizontal and the thickness direction is vertical.

heating rate, the grain structure turns finer and more equi-axed. By combining different rolling practices and heat treatments, a very wide grain size range was achieved for each alloy along the RD: 30 to 750 μm for Alloy-1, 20 to 400 μm for Alloy-2, 18 to 325 μm for Alloy-3, 15 to 225 μm for Alloy-4 and 14 to 130 μm for Alloy-5.

Depending on the Mg level, grain size and testing temperature, both Type A and Type B Lüdering may occur. Lüdering is very common in fully annealed Al-Mg alloys upon tension, while Type A corresponds to a plateau in the yield point and Type B, serrated flow stress after yield point.^[8,9] An increasing Mg level and a decreasing grain size usually make the Lüdering more extensive. As shown in Figure 3, the Lüdering disappears as the temperature reaches 215 °C, while work hardening, not until ~ 300 °C. The YS values as a function of testing temperature in Alloys-1 to 5 with different grain sizes are shown in Figure 4. It can be summarized that

- The YS increases significantly with the increasing Mg in the whole temperature range.
- At room temperature, the YS is greatly dependent on the grain sizes in Alloy-4 and -5, where the Mg levels are high and the grain sizes are small.
- When the Mg levels are low and the grain structures are coarse, *e.g.*, in Alloy-1 and -2, the YS appears less affected by the grain size.
- The grain size effect decreases with the increasing temperature for all the alloys.

IV. DATA ANALYSES

A. Solid Solution Hardening

In Figure 5, the YS is plotted as a function of the inverse square root of grain size. At all temperatures, all the alloys obey the conventional Hall–Petch equation:

$$\sigma = \sigma_0 + \lambda d^{-\frac{1}{2}}, \quad [1]$$

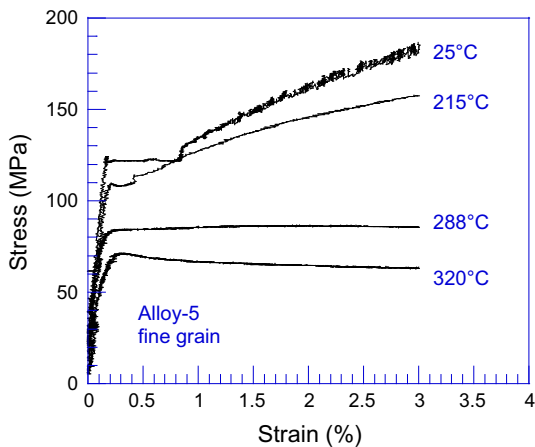


Fig. 3—The tensile curves of fine-grained Alloy-5 tested at 25 °C, 215 °C, 288 °C, and 320 °C.

where σ is the yield stress, σ_0 is the frictional stress which is independent of grain size, λ is the Petch slope, and d is the mean grain size.^[14,15] The values of σ_0 and λ derived by curve fitting are listed in Table II.

When the frictional stress, σ_0 , is plotted against temperature T , a transition temperature around 200 °C is found (Figure 6). Below the transition temperature σ_0 is independent of temperature, while above it σ_0 drops linearly. When the solute level is not very high, the σ_0 and the solute Mg level usually have a linear relationship:

$$\sigma_0 = \sigma_{00} + mc_{\text{Mg}}, \quad [2]$$

where σ_{00} is a frictional stress excluding the effect of Mg, m is a solid solution factor for solution hardening, and c_{Mg} is the atomic fraction of Mg in solid solution. By plotting the σ_0 against c_{Mg} , *e.g.*, see Figure 7, the frictional stress σ_{00} and m factor can be derived (Table III). The Mg in chemical composition is assumed to be all in solid solution.

Figure 8 shows the frictional stress σ_{00} as a function of temperature. Again, it indicates a transition at around 200 °C, below which σ_{00} is independent of temperature and above which σ_{00} drops linearly. When the m factor is plotted against temperature, the values from 177 °C to 260 °C appear to have a large scattering (Figure 9). However, it could be roughly assumed that below the transition temperature, m is less affected by temperature, while above it, a linear relationship exists.

B. Grain Boundary Hardening

The Petch slope λ can be separated into a term independent of solid solution Mg and a term proportional to it:

$$\lambda = \lambda_0 + kc_{\text{Mg}} \quad [3]$$

where λ_0 is the term independent of Mg and k is another solid solution factor, but for grain boundary hardening. In Figure 10, the Petch slope λ is plotted as a function of temperature. The λ drops quickly above the transition temperature, but not perfectly linearly. Below the transition, the λ slightly increases with the increasing temperature, or, it can also be considered nearly temperature independent. By plotting the λ vs c_{Mg} , *e.g.*, see Figure 11, the term independent of solid solution Mg, λ_0 , and the solid solution factor, k , are derived and listed in Table III.

As shown in Figure 12, below the transition temperature λ_0 can roughly be considered constant, while above it λ_0 decreases with the increasing temperature. When the values of λ_0 above 177 °C are plotted vs temperature, a nearly perfect linear relationship is obtained:

$$\lambda_0 = \lambda_{00} + C_\lambda T, \quad [4]$$

where λ_{00} is a temperature-independent term equal to 190 $\text{MPa } \mu\text{m}^{1/2}$ and C_λ is a constant equal to $-0.275 \text{ MPa } \mu\text{m}^{1/2} \text{ K}$. It should be noted that the temperature T is in Kelvin, not Celsius, in all

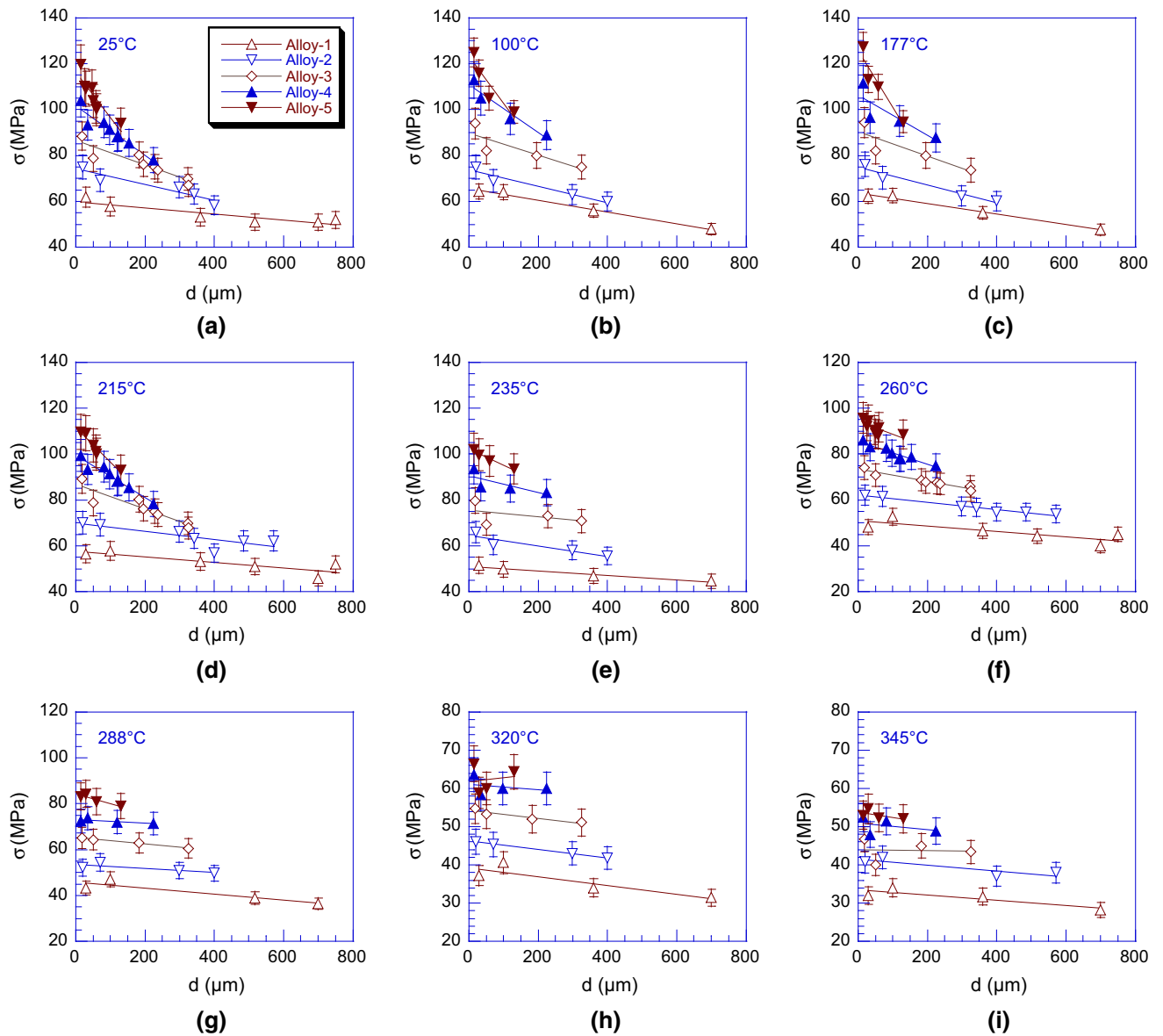


Fig. 4—The yield stress σ as a function of mean grain size d , tested at (a) 25 °C, (b) 100 °C, (c) 177 °C, (d) 215 °C, (e) 235 °C, (f) 260 °C, (g) 288 °C, (h) 320 °C, and (i) 345 °C.

equations hereinafter. In Figure 13, the solid solution hardening factor k is plotted against temperature. Again, there is a transition point at ~ 200 °C, above which k decreases with the increasing temperature, but not very linearly. If the k factor is plotted vs $\frac{1}{T}$ in Figure 14, approximately a linear relationship is obtained:

$$k = k_0 + \frac{C_k}{T} \quad [5]$$

where k_0 is a temperature-independent term equal to -1.59×10^4 MPa $\mu\text{m}^{1/2}$, and C_k is a constant equal to 8.71×10^6 MPa $\mu\text{m}^{1/2}$ K. It should be noted that the k factor becomes negative at above ~ 300 °C.

V. DISCUSSION

Compared to other face-centered-cubic metals, such as copper and silver, aluminum has a low melting point, and its strength is very sensitive to impurity elements.^[16–18] Room temperature, which is usually considered as a low temperature, is nearly 1/3 of the melting point for aluminum. Carreker and Hibbard^[16] have investigated the tensile properties of 99.975 and 99.987 pct pure aluminum from 20 K to 873 K. As shown in Figure 15, the YS decreases continuously with the increasing temperature until reaching a very low value when the temperature is close to the melting point. The slopes of decreasing YS between ~ 100 K and ~ 400 K appear less steep than the ones at lower or higher

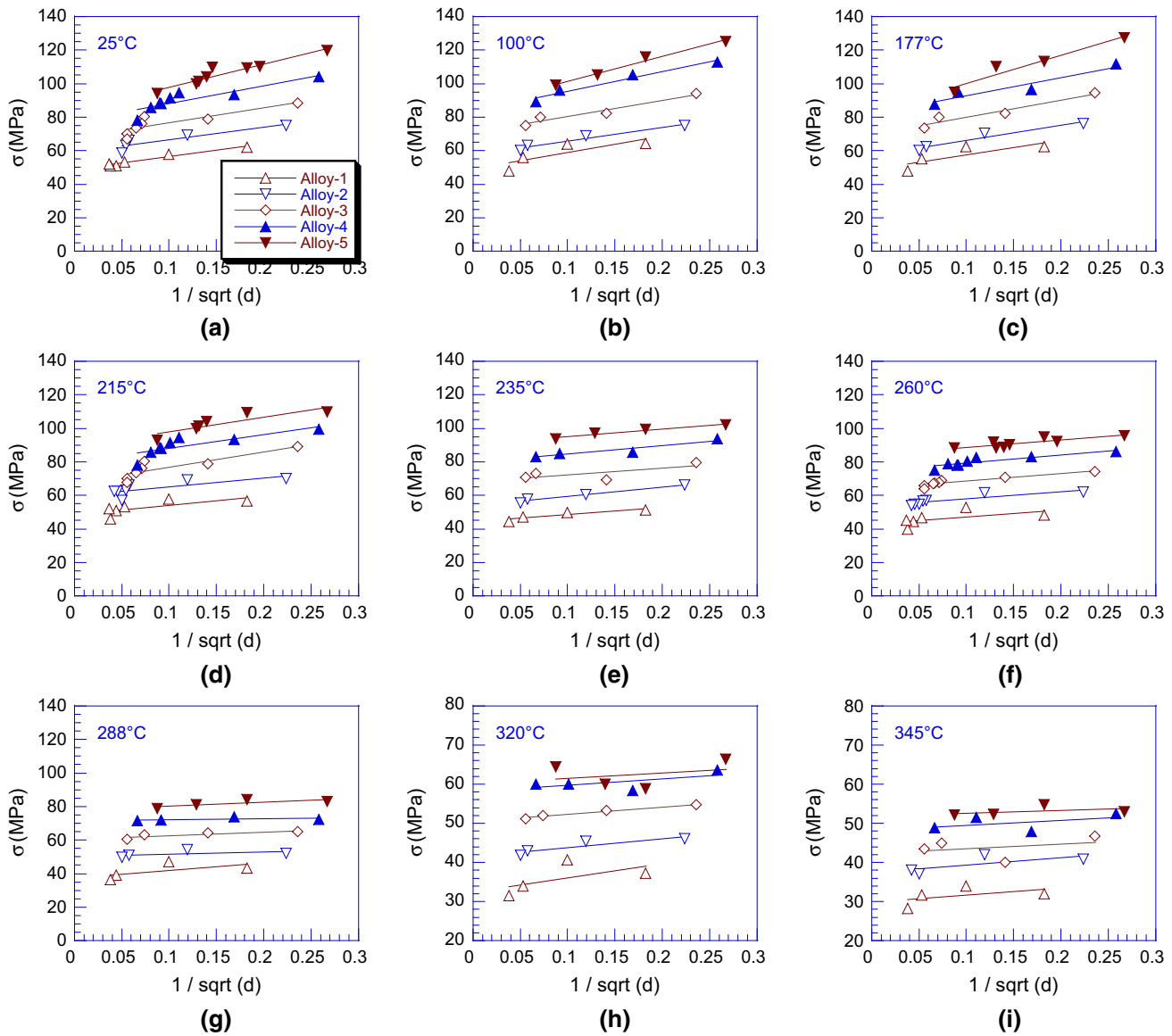


Fig. 5—The frictional stresses as a function of the inverse square root of mean grain sizes, tested at (a) 25 °C, (b) 100 °C, (c) 177 °C, (d) 215 °C, (e) 235 °C, (f) 260 °C, (g) 288 °C, (h) 320 °C, and (i) 345 °C.

Table II. The Values of σ_0 and λ in Hall–Petch Relationship Derived from Fig. 5

T (°C)	Alloy-1		Alloy-2		Alloy-3		Alloy-4		Alloy-5	
	σ_0	λ	σ_0	λ	σ_0	λ	σ_0	λ	σ_0	λ
25	48.8	76.1	58.8	75.6	67.3	89.3	77.6	105.0	84.0	137.8
100	49.0	98.0	57.6	80.8	70.8	95.0	83.4	118.9	86.5	148.2
177	48.8	86.9	57.3	89.0	69.7	101.8	81.7	109.6	83.3	167.9
215	48.7	52.9	59.9	52.1	67.6	91.7	79.9	82.1	89.1	88.0
235	44.2	43.5	53.9	55.1	68.2	40.1	79.6	49.8	90.5	45.7
260	42.9	43.0	53.6	43.0	63.9	45.5	74.2	49.6	84.3	44.2
288	37.5	43.7	50.5	12.2	60.6	21.1	71.5	6.4	77.9	24.0
320	32.4	36.8	41.5	22.6	50.4	18.9	58.0	16.8	59.9	14.6
345	29.8	18.1	37.3	19.7	42.3	11.8	48.3	12.4	51.9	6.9

The units are MPa for σ_0 and MPa $\mu\text{m}^{1/2}$ for λ .

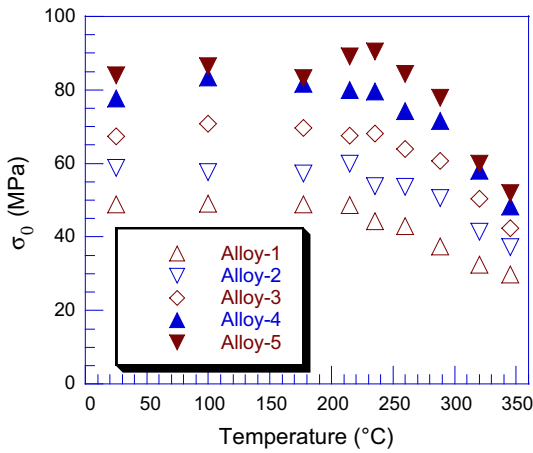


Fig. 6—The frictional stress as a function of temperature.

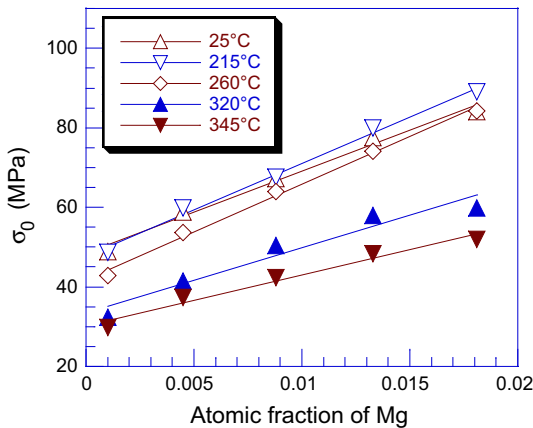


Fig. 7—The frictional stress as a function of Mg in solid solution.

temperatures, especially for the less pure 99.975 pct aluminum. The phenomenon was explained by Carreker and Hibbard as a consequence of strain aging effect from trace amount of impurities. Strain aging is due to impurity locking, most commonly the solute pinning, of dislocations.^[19]

A. Solid Solution Hardening

The solid solution hardening as a function of temperature has been studied in stainless steels, nickel based alloys, silver based alloys, aluminum single crystals, and other metals in relatively low-temperature ranges.^[20–24] From a low temperature close to 0 K to a transition point, usually well below room temperature except for metals with very high melting points, the strength decreases significantly with the increasing temperature. Afterward, there is often a plateau over a large temperature range, where the strength is little affected by temperature. The solid solution hardening, σ_{ss} , is therefore considered to consist of a temperature-dependent term and an athermal term:

$$\sigma_{ss} = \sigma_T + \sigma_T^*, \quad [6]$$

where σ_T is the temperature-dependent term and σ_T^* , the athermal term. The temperature-dependent term is

$$\sigma_T = \frac{k_T}{4} \bar{M} G \varepsilon c \quad [7]$$

where k_T is a factor, \bar{M} is the average Taylor factor, G is the shear modulus, ε is the lattice misfit, and c is the atomic fraction of solutes. The athermal term, on the other hand, can be expressed in many different equations, for example:

$$\sigma_T^* = \frac{k_T^*}{4} \bar{M} G (\varepsilon c)^{\frac{4}{3}}, \quad [8]$$

where k_T^* is another factor.^[19] The athermal term σ_T^* is usually much smaller than σ_T and different equations often yield similar values.

As shown in Figure 6, from room temperature to ~200 °C, the frictional stress independent of grain size is nearly constant, while from ~200 °C to 345 °C, it decreases linearly. Since the melting point of aluminum is very low, the current study is performed in a quite high-temperature range, different from References 20 through 24. In Reference 23, the solid solution hardening in highly pure aluminum single crystals with 0.6 to 9.0 at. pct Mg was studied from 1.6 K to 300 K by tensile testing at $7 \times 10^{-4} \text{ s}^{-1}$ constant strain rate, covering the low-temperature range omitted in the current study. It was found that from 1.6 K to ~25 K, there is an anomaly that the shear stress increases with the increasing temperature. The stress drops significantly from ~25 K to ~125 K, followed by a plateau up to 300 K, e.g., see Figure 16, where the shear stress data with 0.6, 1.6, and 2.0 at. pct Mg are re-plotted.

In Figure 17, the yield stress of aluminum single crystal with 0.6 at. pct Mg from Reference 23 and the frictional stress σ_0 independent of grain boundary hardening of Alloy-2, containing 0.45 at. pct Mg, are plotted together as a function of temperature. Modifications have been done to the data from Reference 23. First, as the orientation of the single crystal is unclear, the shear stress, τ , was converted roughly to the yield stress σ_0 by multiplying it with the average Taylor factor \bar{M} , 3.06. Second, an offset of 40 MPa covering the hardening effects from Mn, Cu, and impurity and additive elements, which will be discussed in detail later, was added. Although Figure 17 shows merely a very rough combination, four stages can easily be identified: Stage I—Anomaly, Stage II—Steep decrease, Stage III—Plateau, and Stage IV—Second steep decrease. Beyond Stage I, the strength follows a monotonic decreasing tendency with the increasing temperature. For the current study, the data from room temperature to ~200 °C form part of Stage III, and the data above ~200 °C, part of Stage IV.

Stages I and II are not the focus of the current study. The anomaly in Stage I has been explained by quantum effects or structural changes in slip bands at temperatures near 0 K.^[25,26] The monotonic decreasing from Stage II to Stage IV is controlled by the thermal activation-induced mobility, or, diffusivity, of solute

Table III. The Frictional Stress σ_{00} and Solid Solution Hardening Factor m Derived from Fig. 7, the Term Independent of Solid Solution Mg, λ_0 , and the Solid Solution Hardening Factor k Derived from Fig. 11

T (°C)	σ_{00} (MPa)	m (MPa)	λ_0 (MPa $\mu\text{m}^{1/2}$)	k (MPa $\mu\text{m}^{1/2}$)
25	48.5	2.06×10^3	63.7	3.62×10^3
100	48.2	2.33×10^3	77.8	3.33×10^3
177	48.5	2.15×10^3	71.4	4.34×10^3
215	47.7	2.34×10^3	52.3	2.30×10^3
235	42.2	2.74×10^3	47.2	-0.04×10^3
260	41.9	2.40×10^3	43.2	0.20×10^3
288	38.1	2.35×10^3	30.2	-0.96×10^3
320	33.4	1.64×10^3	32.3	-1.13×10^3
345	30.3	1.27×10^3	20.2	-0.70×10^3

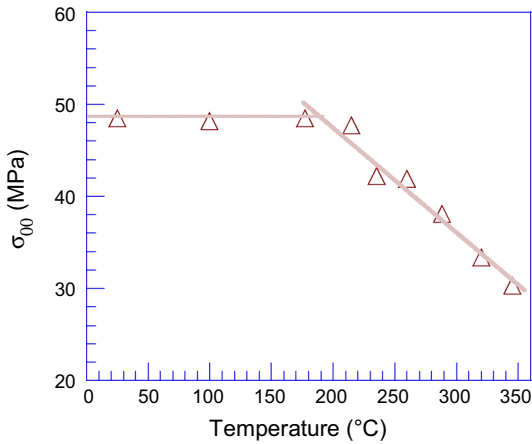


Fig. 8—The frictional stress excluding the effect of Mg as a function of temperature.

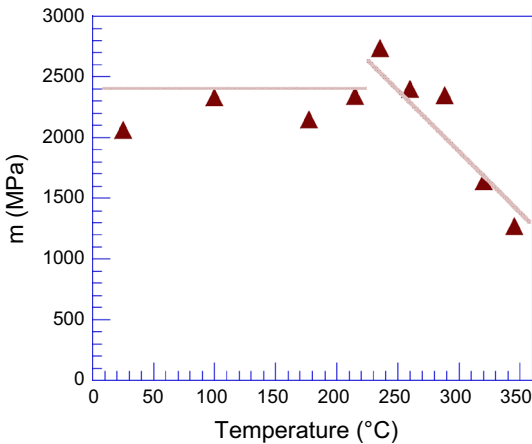


Fig. 9—The solid solution factor m for solution hardening as a function of temperature.

elements, majorly Mg. The lattice diffusivity, D , as a function of temperature is given by

$$D = D_0 \exp\left(\frac{-Q}{RT}\right), \quad [9]$$

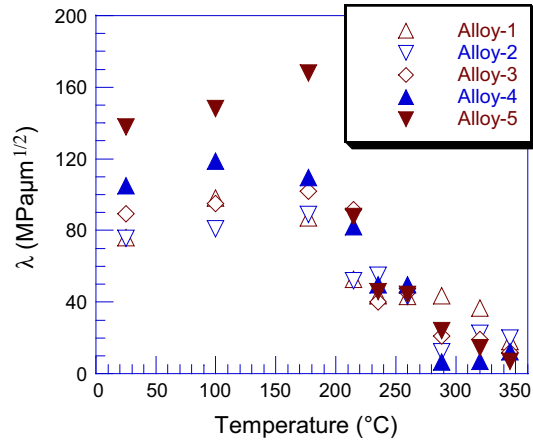


Fig. 10—The Petch slope as a function of temperature.

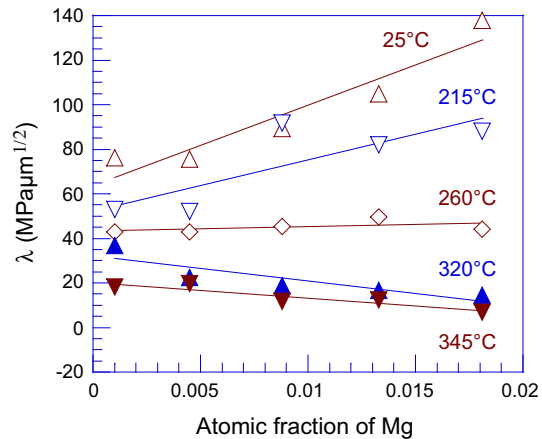


Fig. 11—The Petch slope as a function of Mg in solid solution.

where D_0 is the preexponential factor, Q is the activation energy, and R is the gas constant equal to $8.314 \text{ Jmol}^{-1} \text{ K}^{-1}$. Depending on the methodologies of measurement and calculation, the values of D_0 and Q vary in a very wide range. For Mg, Mn, and Cu in aluminum, generally it is accepted that the diffusivity of Mg is the highest, that of Cu is somewhat lower, while that of Mn is extremely low. Some moderate and

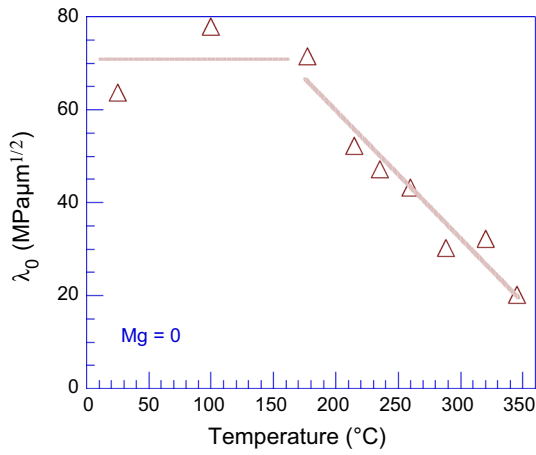


Fig. 12—The Petch slope independent of Mg as a function of temperature.

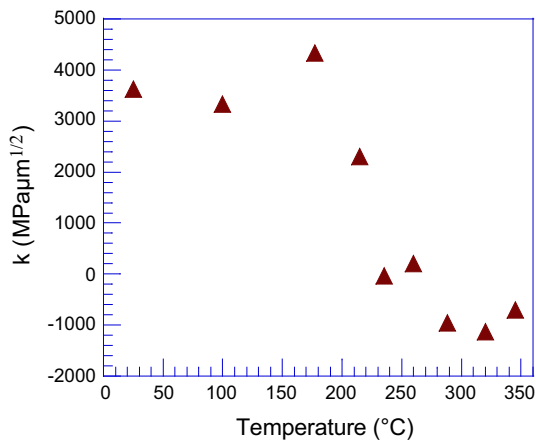


Fig. 13—The solid solution factor k for grain boundary hardening as a function of temperature.

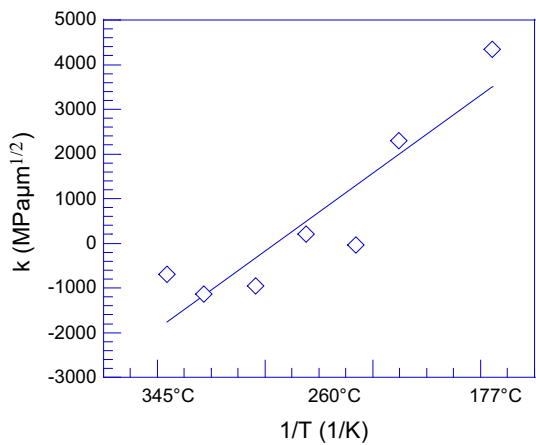


Fig. 14—The k factor vs inverse temperature $\frac{1}{T}$ in the range from 177 °C to 345 °C.

reasonable values of D_0 and Q for Mg, Mn, and Cu are listed in Table IV.^[27–29] Based on these values, the diffusivities are calculated as a function of temperature from Eq. [9] (Figure 18).

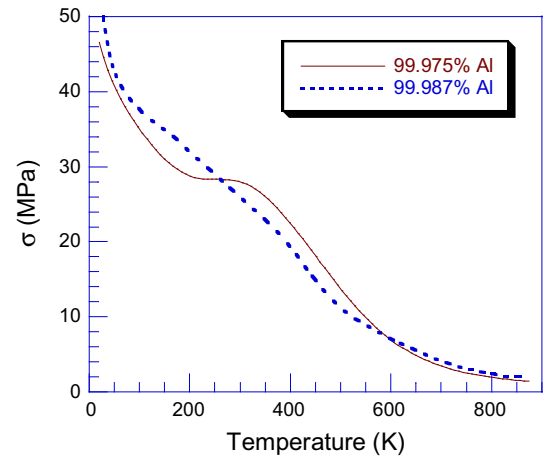


Fig. 15—The yield stresses of 99.975 and 99.987 pct pure aluminum as a function of temperature, re-plotted from Ref. [16]. The mean grain size is 113 μm for the 99.975 pct aluminum and 46 μm for the 99.987 pct one.

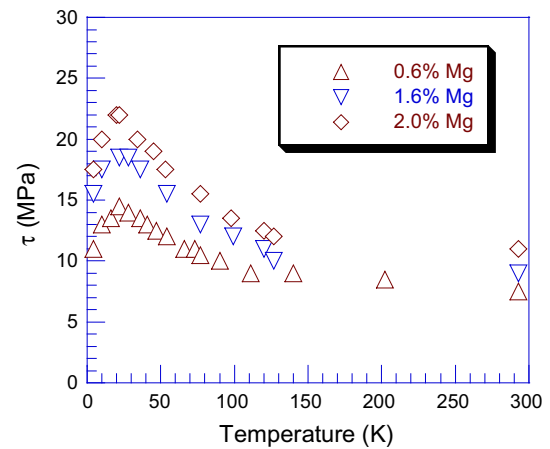


Fig. 16—The shear stress in aluminum single crystals with 0.6, 1.6, and 2.0 at. pct Mg as a function of temperature, re-plotted from Ref. [23].

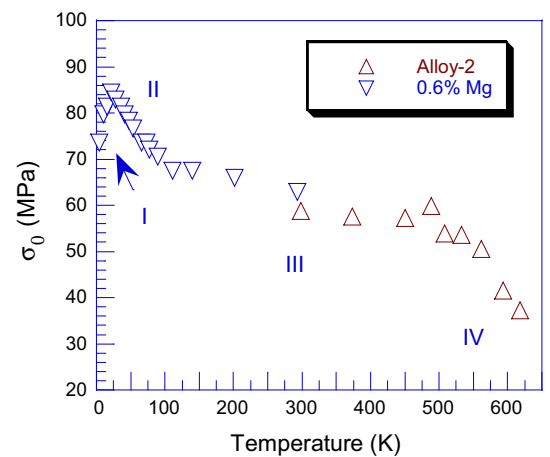


Fig. 17—The strength of aluminum single crystal with 0.6 at. pct Mg from Ref. [23] and the frictional stress of Alloy-2 with 0.45 at. pct Mg, as a function of temperature.

Table IV. The Values of Preexponential Factor D_0 and Activation Energy Q for Mg, Mn, and Cu in Aluminum

T (°C)	Mg	Mn	Cu
D_0 (m^2s^{-1})	6.6×10^{-5}	8.7×10^{-3}	6.54×10^{-5}
Q (kJ mol^{-1})	124.5	208.0	136.0

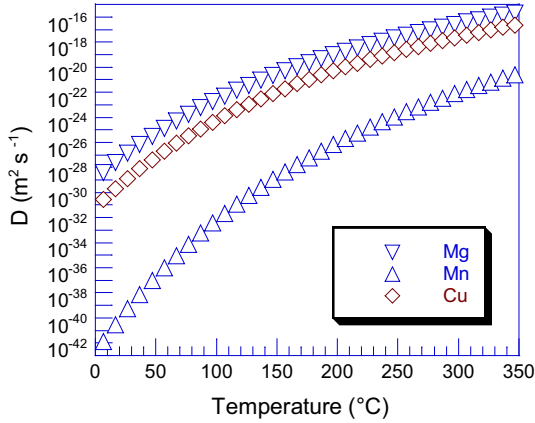


Fig. 18—The lattice diffusivities of Mg, Mn, and Cu in aluminum as a function of temperature.

In Stage II, where temperature is sufficiently low such that diffusional recovery is hard to occur, the Mg solutes can be considered as uniformly distributed immobile impurities. The hardening effect is thus determined by lattice misfit ε , solute concentration c_{Mg} , and the shear modulus G which decreases nearly linearly with the increasing temperature. In Stage III, the mobility of Mg solutes is high enough to form the Cottrell clouds, which increase the solute-pinning effect on dislocations dramatically. The enhanced solute pinning compensates the effect of decreasing shear modulus, leading to the plateau in stress–temperature curve. Sometimes, the enhanced solute pinning can even raise the curve slightly.

Type B Lüdering is an indication of the enhanced solute pinning by Cottrell clouds, where pinning, break-away, and re-pinning happen alternatively and continuously.^[30,31] As shown in Figure 3, at 215 °C, the Lüdering starts to disappear, indicating that ~ 200 °C is a transition point from Stage III to Stage IV. In Stage IV, the mobility of Mg solutes is so high that the Cottrell clouds diffuse easily with the moving dislocations, generating some dragging, but are unable to catch and re-pin the dislocations, or, the clouds evaporate readily. Both result in drastic decrease of solute pinning effect and consequently the steep drop of strength.

Although the solid solution hardening in Stage III is often expressed by the athermal term σ_T^* (Eq. [8]), for aluminum alloys, it is more common and convenient to use the temperature-dependent term σ_T (Eq. [7]) but fixing the shear modulus G at the room temperature value, to be 26.0 GPa. It is difficult to measure the shear moduli accurately through the whole temperature range,

Table V. The Shear Modulus G , the Solid Solution Hardening per 1 Atomic Percent Mg, $\Delta\sigma_T$, Calculated by Eq. [7], and the Experimental Values from 25 °C to 345 °C

T (°C)	G (GPa)	$\Delta\sigma_T$ (MPa)	Experimental (MPa)
25	26.0	23.9	20.6
100	24.8	22.8	23.3
177	23.8	21.9	21.5
215	23.0	21.1	23.4
235	22.7	20.8	27.4
260	22.4	20.6	24.0
288	21.8	20.0	23.5
320	21.4	19.7	16.4
345	20.8	19.1	12.7

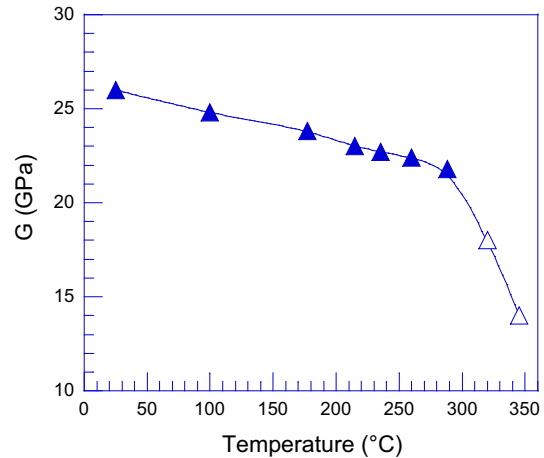


Fig. 19—The shear moduli at 25 °C to 345 °C derived from Refs. [32] through [34] but adjusted by the experimental data of the current study.

but there are some reasonable experimental data available for pure aluminum.^[32–34] In general, the shear modulus exhibits a linear behavior from very low temperature near 0 K to ~ 375 °C, while afterward, it drops drastically due to grain boundary relaxation.^[35]

In Table V, the contribution of solid solution hardening per 1 at. pct Mg (c_{Mg} is 0.01), $\Delta\sigma_T$, is calculated at different temperatures from Eq. [7]. In the calculation, the k_T is assumed to be 1, \bar{M} is 3.06, the temperature-dependent G values are taken from References,^[32–34] and lattice misfit ε is 0.12. For comparison, the experimentally determined values per 1 at. pct Mg are also listed in Table V. The calculated and experimental values are very close except for the very high-temperature range above 300 °C, indicating that Eq. [7] is valid in both Stage III and Stage IV. The overestimation of the calculated solution hardening at above 300 °C is likely due to the uncertainty of shear moduli in high-temperature range. For example, the grain boundary relaxation may start in Al-Mn-Cu-Mg alloys at ~ 300 °C, rather than ~ 375 °C which was determined in pure aluminum. In Figure 19, the shear moduli at 25 °C to 345 °C derived from References 32 through 34 are adjusted by the experimental data of the current study.

B. Frictional Stress and Grain Boundary Hardening

In the current study, the frictional stress term σ_{00} consists of not only the true frictional stress of pure aluminum, but also the dispersion hardening from $\text{Al}_6(\text{Mn,Fe})$ and the solution hardening from Mn, Cu and other trace elements. The true frictional stress of pure aluminum is 10 MPa and the dispersion hardening is usually very weak in regular aluminum alloys, for high-Mn aluminum alloys, 2 to 5 MPa. The solid solution hardening is ~ 145 MPa per wt pct for Mn and ~ 15 MPa per wt pct for Cu, while the room temperature solubility is below 0.1 wt pct for Mn and ~ 0.3 wt pct for Cu.^[8] However, the specimens in the current study are in supersaturated condition, since the ingots were re-heated at 520 °C without formal homogenization, which is ~ 600 °C for most Al-Mn alloys, and the specimens were quenched after annealing. Under this condition, the solute level is at least 0.14 wt pct for Mn, leading to more than 20 MPa, and ~ 0.5 wt pct for Cu, leading to ~ 8 MPa.^[8] Moreover, the alloys contain impurity elements, mainly ~ 0.25 wt pct Fe and ~ 0.1 wt pct Si, and trace amount of additive elements, *i.e.*, Ti and B from grain refiner. It is reasonable to assume that the contribution from Mn, Cu, and other trace elements is close to 40 MPa, making the room-temperature frictional stress σ_{00} to be around 48.5 MPa.

The plateau of the frictional stress between 25 °C and ~ 200 °C shown in Figure 8 is likely due to the enhanced solute pinning from Mn, Cu, and possibly other trace elements, especially the Cu. The Mn has not only very small solubility but also very low diffusivity (Figure 18), so it cannot form Cottrell clouds. On the contrary, Cu is able to form Cottrell clouds, since it has moderate solubility and quite high diffusivity (Figure 18), and serrated tensile flow at room temperature has been observed in some Al-Cu alloys. Actually, the formation of Cottrell clouds is not very necessary for enhanced solute pinning. Whenever solutes are able to segregate to dislocations, more effective pinning occurs, and the hardening becomes stronger than regular discrete obstacle pinning.^[27]

Above the transition temperature σ_{00} is dominated by Mn and Cu solutes, especially the Cu, since the true frictional stress of pure aluminum and dispersion hardening are even smaller at elevated temperatures. Supposing the solution hardening from Cu is the same as that from Mg in Stage IV, *e.g.*, the extensive segregation of Cu solutes to dislocations disappears due to the very high solute mobility, the solute hardening is controlled by the temperature-dependent shear modulus. A frictional stress linearly decreasing with the increasing temperature from ~ 200 °C up to 345 °C is therefore natural. When the values of σ_{00} above 177 °C in Figure 8 are plotted against temperature, a linear relationship is derived:

$$\sigma_{00} = 100 - 0.11T \quad [10]$$

For grain boundary hardening, there are two fundamental theories: the one due to dislocation pile-up^[14,15,36,37] and the other due to work hardening

from geometrically necessary dislocations,^[38] both leading to the same form of Hall–Petch relationship. Other theories or models are more or less based on or modified from the two fundamental theories. An overview of the different theories and models is available in Reference 39. Using the basic concept of pile-up theory, the Petch slope can be expressed in a general and simple form as follows:

$$\lambda = \alpha G b^{\frac{1}{2}}, \quad [11]$$

where α is a constant dependent on chemistry and microstructure/texture, and b is the Burger's vector. For pure aluminum, these values are ~ 0.2 and 2.86 Å, respectively, and accordingly at room temperature, the λ is 80 MPa $\mu\text{m}^{1/2}$.^[39]

The values of λ_0 from 25 °C to 177 °C in Table III, ranging from 64 to 78 MPa $\mu\text{m}^{1/2}$, are very close to the theoretical value of 80 MPa $\mu\text{m}^{1/2}$ for pure aluminum. However, although λ_0 is independent of solute Mg, the effects of Mn and Cu solutes are not negligible. It is well accepted that the Petch slope is very sensitive to the solution-hardening elements, such as nitrogen and carbon in steels.^[20,40] According to Eq. [11], the Petch slope should linearly decrease with the increasing temperature, since the shear modulus is roughly a linear function of temperature. However, Figures 10 and 12 reveal that a plateau exists below the transition point at ~ 200 °C. Such a plateau is likely due to the solutes, which provide enhanced pinning on the dislocations near or at grain boundaries,^[15,37] the same as that for frictional stress.

The solute strengthening of grain boundaries is very complicated, and there is no solid conclusion yet. It was proposed that solute carbon increases the Petch slope by influencing the unpinned stress to locked dislocations.^[41,42] For nitrogen in stainless steels, it is more complex. The nitrogen atoms promote planar arrays of dislocations and also increase the stacking fault energy.^[20] Compared to steels, the Petch slope is small for most aluminum alloys except Al-Mg alloys.^[9] Based on the fundamental pile-up theory, the flow stress is the external stress which creates a critical stress concentration at a certain distance ahead of the pile-up. The critical stress concentration should be able to unpin a dislocation source near or at the grain boundary.^[15,37] Whenever the dislocation sources are more strongly locked, *e.g.*, by extensive segregation of solutes, the critical stress concentration required to unpin increases, leading to a higher Petch slope. Regardless of the details, when the solute level is relatively dilute, the linear function, *i.e.*, $\lambda = \lambda_0 + kc_{\text{Mg}}$, is the simplest but reasonable expression.

Although λ_0 is independent of Mg, it is affected by the other solute elements, mainly Cu. Above the transition point at ~ 200 °C, the extensive segregation of solutes to dislocations, *e.g.*, Cottrell clouds, disappears, and the solute pinning is controlled by the shear modulus. Consequently, the Petch slope becomes linearly dependent on temperature, as shown in Eq. [12], due to the linear relationship between the shear modulus and temperature. Although several expressions for the Petch

slope, such as the strain level, may be involved, the Burger's vector term could be written as b instead of $b^{\frac{1}{2}}$; the shear modulus G term is seldom changed. Therefore, Eq. [4], $\lambda_0 = \lambda_{00} + C_\lambda T$, is valid regardless of the details of the grain boundary hardening mechanisms.

The theoretical physics behind Eq. [5], $k = k_0 + \frac{C_k}{T}$, depends on the concept of equi-cohesive temperature. Above the equi-cohesive temperature, the grain boundaries are weaker, not stronger, than the grain interiors.^[43,44] It is not surprising that the grain boundary hardening diminishes quickly with the increasing temperature. At elevated temperatures, grain boundary relaxation makes dislocations move across grain boundaries or the dislocation sources become unpinned more easily. As shown in Figure 15, when approaching the melting point, the strength drops to and stabilizes at a very small value. Equation [5] with a term of $\frac{1}{T}$ may not be ideally the best, but is the simplest, to represent such a tendency. When approaching the equi-cohesive temperature, the Mg solutes effectively soften the grain boundaries, leading to negative k values.

C. Semiempirical Expressions

There are five fundamental strengthening mechanisms in aluminum alloys: solid solution, grain boundary, precipitation, dispersion, and work hardening. In the current study, no work hardening or precipitation hardening was involved. The chemical compositions except Mg, casting condition, and the sheet-processing route, which determine the phase, number, size, and spatial distribution of dispersoids, are identical for the five alloys. The subsequent heat treatments for different grain sizes should not affect the dispersion hardening, since the volume fraction and particle size of $Al_6(Mn,Fe)$ phase can only be changed after exposure at homogenization temperature, 540 °C to 600 °C, for several hours. The dispersion hardening, which is usually very weak in aluminum alloys, is therefore considered a constant.

The solid solution hardening from Mg and the grain boundary hardening are the only variables. All the other strengthening variables, *e.g.*, dispersion hardening and solid solution hardening from Mn, Cu, and possibly other elements, can be allocated to the frictional stress term σ_{00} , *i.e.*,

$$\sigma = \sigma_{00} + \sigma_{ss} + \sigma_{gb}, \quad [12]$$

where σ_{ss} is the solid solution hardening from Mg and σ_{gb} is the grain boundary hardening. Attributed to the enhanced solute pinnings of Mg, Mn, and Cu on the dislocations, the values of σ_{00} , σ_{ss} , and σ_{gb} appear nearly constant from room temperature to the transition point at ~ 200 °C (Figures 8 to 10).

Since the solid solution hardening from Mg, σ_{ss} , is given by $\frac{1}{4}\bar{M}G\epsilon c_{Mg}$, and the grain boundary hardening, σ_{gb} , is given by $\lambda d^{-\frac{1}{2}}$, where λ is $\lambda_0 + kc_{Mg}$, the yield stress can be expressed in a general form:

$$\sigma = \sigma_{00} + \frac{1}{4}\bar{M}G\epsilon c_{Mg} + (\lambda_0 + kc_{Mg})d^{-\frac{1}{2}} \quad [13]$$

At room temperature, σ_{00} is 48.5 MPa, $\frac{1}{4}\bar{M}G\epsilon$ is 2.4×10^3 MPa, λ_0 is 70 MPa $\mu m^{1/2}$, and k is 3.8×10^3 MPa $\mu m^{1/2}$, giving a semiempirical expression for temperatures from 25 °C to ~ 200 °C:

$$\sigma = 48.5 + 2.4 \times 10^3 c_{Mg} + (70 + 3.8 \times 10^3 c_{Mg})d^{-\frac{1}{2}} \quad [14]$$

When Eqs. [4], [5], [7], and [10] are integrated into Eq. [13], another semiempirical expression is obtained for ~ 200 °C to 345 °C:

$$\sigma = (100 - 0.11T) + 0.09Gc_{Mg} \left\{ (190 - 0.275T) + \left(-1.59 \times 10^4 + \frac{8.71 \times 10^6}{T} \right) c_{Mg} \right\} d^{-\frac{1}{2}} \quad (15)$$

where G can be taken from Figure 19. It should be noted that the units of G , T and d are MPa, K and μm , respectively, in the equations.

VI. CONCLUSION

In the temperature range from 25 °C to 345 °C, there is a transition around 200 °C for Al-1.5wt pctMn-0.5wt pctCu alloys with up to 2.1 wt pct Mg. Below the transition point, the frictional stress, solid solution hardening from Mg and grain boundary hardening are little affected by temperature, due to enhanced solute pinning on dislocations. The enhanced solute pinning from Mg and Cu is attributed to Cottrell clouds, while those from Mn and other elements are unclear, possibly due to other extensive segregation of solutes toward dislocations. Above the transition, the solid solution hardening is controlled by the temperature-dependent shear modulus, which decreases linearly with the increasing temperature up to ~ 300 °C. Therefore, both the frictional stress and the solution hardening from Mg decrease linearly with the increasing temperature above ~ 200 °C.

The grain boundary hardening obeys the Hall-Petch equation in the whole temperature range. Below the transition point the Petch slope is mainly controlled by the solute Mg, while above the point it is dependent on both solute Mg and temperature. The Petch slope increases linearly with the solute Mg level, and decreases proportionally with the inverse temperature. Semiempirical expressions for the yield stress were derived, including both the solid solution and grain boundary effects: $\sigma = 48.5 + 2.4 \times 10^3 c_{Mg} + (70 + 3.8 \times 10^3 c_{Mg})d^{-\frac{1}{2}}$ for 25 °C to ~ 200 °C, and $\sigma = (100 - 0.11T) + 0.09Gc_{Mg} + \left\{ (190 - 0.275T) + \left(-1.59 \times 10^4 + \frac{8.71 \times 10^6}{T} \right) c_{Mg} \right\} d^{-\frac{1}{2}}$ for ~ 200 °C to 345 °C.

ACKNOWLEDGMENTS

The permission given by the Natural Resources Canada to publish the current study is gratefully acknowledged. The funding was provided by the Natural Resources Canada through the Program of Energy Research and Development. We express our appreciation for the valuable discussions with Dr. D.J. Lloyd.

REFERENCES

1. G.E. Totten and D.S. MacKenzie: *Handbook of Aluminum: Volume 2: Alloy Production and Materials Manufacturing*, CRC Press, Boca Raton, 2003.
2. O.D. Sherby, R.A. Anderson, and J.E. Dorn: *Trans. AIME*, 1951, vol. 191, pp. 643–52.
3. T.E. Mitchell: *Encycl. Mater. Sci. Technol.*, 2001, vol. 10, p. 9827.
4. Ø. Ryen, O. Nijs, E. Sjölander, B. Holmerdal, H.-E. Ekström, and E. Nes: *Metall. Mater. Trans. A*, 2006, vol. 37A, pp. 1999–2006.
5. D.O. Sprowls and R.H. Brown: *Fundamental Aspects of Stress Corrosion Cracking*, National Association of Corrosion Engineers, Houston, 1969, pp. 466–512.
6. A.F. Beck and P.R. Sperry: *Fundamental Aspects of Stress Corrosion Cracking*, National Association of Corrosion Engineers, Houston, 1969, pp. 513–29.
7. M.O. Speidel, and M.V. Hyatt: *Advances in Corrosion Science and Technology*, vol. 2, M.G. Fontana, and R.W. Staehle, Plenum Press, New York, NY, 1972, pp. 115–55.
8. S.A. Court, K.M. Gatenby, and D.J. Lloyd: *Mater. Sci. Eng.*, 2001, vols. A319–A321, pp. 443–47.
9. D.J. Lloyd and S.A. Court: *Mater. Sci. Technol.*, 2003, vol. 19, pp. 1349–54.
10. G.J. Marshall, R.K. Bolingbroke, and A. Gray: *Metall. Mater. Trans. A*, 1993, vol. 24A, pp. 1935–42.
11. G.J. Marshall, A.J.E. Flemming, A. Gray, and R. Llewellyn: *Proceedings of the 4th International Conference on Aluminium and Alloys*, Atlanta, USA, 1994, vol. 1, pp. 467–74.
12. H. Jin, J. Liang, Y. Zeng, and M.S. Kozdras: *SAE Int. J. Mater. Manuf.*, 2015, vol. 8 (3), pp. 736–43.
13. H. Jin, M.S. Kozdras, B. Shalchi, B.S. Amirkhiz, and S.L. Winkler: *Metall. Mater. Trans. A*, 2018, vol. 49A, pp. 3091–3108.
14. E.O. Hall: *Proc. Phys. Soc. Lond. B*, 1951, vol. 64, pp. 747–55.
15. N.J. Petch: *J. Iron Steel Inst.*, 1953, vol. 174, pp. 25–28.
16. R.P. Carreker and W.R. Hibbard: *JOM*, 1957, vol. 9, pp. 1157–63.
17. R.P. Carreker and W.R. Hibbard: *Acta Metall.*, 1953, vol. 1, pp. 654–63.
18. R.P. Carreker: *JOM*, 1957, vol. 9, pp. 112–15.
19. J. Friedel: *Dislocations*, Pergamon Press, Great Britain, 1964.
20. L.-Å. Norström: *Metal Sci.*, 1977, vol. 11, pp. 208–12.
21. M.M. Hutchison and R.W.K. Honeycombe: *Metal Sci.*, 1967, vol. 1, pp. 70–74.
22. Y. Nakada and A.S. Keh: *Metall. Trans.*, 1971, vol. 2, pp. 441–47.
23. V.P. Podkuyko and V.V. Pustovalov: *Cryogenics*, 1978, vol. 18, pp. 589–95.
24. U.F. Kocks: *Metall. Mater. Trans. A*, 1985, vol. 16A, pp. 2109–2129.
25. P. Feltham: *Phys. Stat. Sol. (b)*, 1980, vol. 98, pp. 301–06.
26. P. Feltham: *Phys. Stat. Sol. (a)*, 1983, vol. 75, pp. K95–98.
27. J. Verlinden and R. Gijbels: *Adv. Mass. Spectrom.*, 1980, vol. 8A, pp. 485–95.
28. G. Rummel, T. Zumkley, M. Eggersmann, K. Freitag, and H. Mehrer: *Z. Metallkd.*, 1995, vol. 86, pp. 122–30.
29. S. Fujikawa and K. Hirano: *Def. Diff. Forum*, 1989, vols. 66–69, pp. 447–52.
30. A.H. Cottrell and B.A. Bilby: *Proc. Phys. Soc. A*, 1949, vol. 62, pp. 49–61.
31. D.J. Lloyd: *Metall. Mater. Trans. A*, 1980, vol. 11A, pp. 1287–94.
32. W. Köster: *Z. Metallkde.*, 1948, vol. 39, pp. 1–9.
33. P.M. Sutton: *Phys. Rev.*, 1953, vol. 91, pp. 816–21.
34. R.B. McLellan and T. Ishikawa: *J. Phys. Chem. Solids*, 1987, vol. 48, pp. 603–06.
35. T-S. Kê: *Phys. Rev.*, 1947, vol. 71, pp. 533–46.
36. R.W. Armstrong, I. Codd, R.M. Douthwaite, and N.J. Petch: *Philos. Mag.*, 1962, vol. 7, pp. 45–58.
37. A.H. Cottrell: *Trans. TMS-AIME*, 1958, vol. 212, pp. 192–203.
38. M.F. Ashby: *Philos. Mag.*, 1970, vol. 21, pp. 399–424.
39. Z.C. Cordero, B.E. Knight, and C.A. Schuh: *Int. Mater. Rev.*, 2016, vol. 61, pp. 495–512.
40. V.G. Gavriljuk, H. Berns, C. Escher, N.I. Glavatskaya, A. Sozinov, and Y.N. Petrov: *Mater. Sci. Eng. A*, 1999, vol. 271, pp. 14–21.
41. T.L. Russel, D.S. Wood, and D.S. Clark: *Acta Metall.*, 1961, vol. 9, pp. 1054–63.
42. D.V. Wilson: *Metal Sci.*, 1967, vol. 1, pp. 40–47.
43. W. Rosenhain and D. Ewen: *J. Inst. Metals*, 1913, vol. 10, pp. 119–39.
44. Z. Jeffries: *Trans. AIME*, 1919, vol. 60, pp. 474–576.